Euler-Lagrange Computational Fluid Dynamics Simulation of a Full-Scale Unconfined Anaerobic Digester for Wastewater Sludge Treatment

D. Dapelo and J. Bridgeman
School of Civil Engineering
University of Birmingham, United Kingdom

Abstract

For the first time, an Euler-Lagrange model for Computational Fluid Dynamics (CFD) is used to model a full-scale gas-mixed anaerobic digester. The design and operation parameters of a digester from a wastewater treatment works are modelled, and mixing is assessed through a novel, multi-facetted approach consisting of the simultaneous analysis of (*i*) velocity, shear rate and viscosity flow patterns, (*ii*) domain characterization following the average shear rate value, and (*iii*) concentration of a non-diffusive scalar tracer. The influence of sludge's non-Newtonian behaviour on flow patterns and its consequential impact on mixing quality were discussed for the first time. Recommendations to enhance mixing effectiveness are given: (*i*) a lower gas mixing input power can be used in the digester modelled within this work without a significant change in mixing quality, and (*ii*) biogas injection should be periodically switched between different nozzle series placed at different distances from the centre.

Keywords: wastewater, sludge, CFD, Euler-Lagrangian, non-Newtonian fluid, turbulence, energy.

1 Introduction

This paper considers the Computational Fluid Dynamics (CFD) modelling of a full-scale gas-mixed anaerobic digester. The purpose of this work was to develop recommendations to minimize the input mixing power without compromising, and indeed enhancing, biogas yield for the scenario considered. This was done by progressively lowering the mixing input power while analyzing the resulting flow patterns. This work is based on Dapelo et al. [1], but the current article also includes: (*i*) a systematic assessment of the model mesh-independence through the Grid Convergence Index (GCI) as proposed by [2]; (*ii*) a more complete analysis of the flow patterns by comparison of velocity and viscosity plots; (*iii*) additional simulations to track the distribution of a non-diffusive scalar field to be used as a virtual tracer and to reproduce the Herschel-Bulkley rheology; (*iv*) an analysis of the presence of low-viscosity corridors in the digester, and their detrimental effect on mixing; (*v*) an assessment of a mitigation strategy consisting of abruptly switching biogas injection between two nozzle series at regular intervals; and (*vi*) an alternative approach to calculate the value of minimum power per unit volume necessary for a satisfactory level of mixing computed in the original conference paper is presented here.

Wastewater treatment is an energy-intensive operation. Energy use at wastewater treatment works (WwTWs) which come under the auspices of the Urban Wastewater Treatment Directive (UWwTD) and for which EU Member States returned data exceeds 23,800 GWh per annum[3]. Energy consumption has increased significantly in the last two decades, and further increases of 60% are forecast in the next 10-15 years, primarily due to tightened regulation of effluent discharges from WwTWs (e.g. Water Framework Directive, WFD) [4]. WFD impacts will not be truly appreciated for many years, but the UK water industry forecasts a GBP 100M energy cost increase from implementation of more stringent treatment standards [5]. However, predictions show that by 2030 the world will have to produce 50% more food and energy and provide 30% more water [6], while mitigating and adapting to climate change, threatening to create a "perfect storm" of global events. Therefore, we must address the explicit link between wastewater and energy.

Renewable energy resources development is an integral part of several EU Governments' environmental strategies. Mesophilic anaerobic digestion (MAD) is the most widespread technology for sludge treatment, the by-product of wastewater treatment, in which sludge is mixed with anaerobic bacteria to break down biodegradable material and produce a methane-rich biogas. The current drive to maximise energy recovery means biogas is increasingly harnessed via combined heat and power technology. So, we need to optimise MAD reactor (digester) and mixing performance to maximize energy recovery.

In order to predict confidently optimum digester mixing, we need to determine to what extent biogas output is influenced by flow patterns in a digester; flow patterns which are determined by physical parameters of the digesters, inflow mode, sludge rheology and, crucially, mixing regimes. Yet research is lacking in this area. Traditional approaches to digester design are firmly rooted in empiricism and rule of thumb rather than science, and design standards focus only on treated sludge quality, not quality and gas yield/energy consumption.

Although the importance of thorough mixing has been recognized, recent studies [7, 8, 9, 10, 11], have questioned traditional approaches. A consistent body of literature[15, 16, 17, 18, 14, 12, 13, 19, 20] has shown that computational fluid dynamics (CFD) offers significant potential for understanding flow patterns of the non-Newtonian sewage sludge within digesters. However, there are clear limitations with the work undertaken to date; for example, while much work has been done to understand mechanical mixing, gas mixing remains poorly studied.Although it is recognized that mechanical mixing is the most efficient mode of mixing [21, 14], gas mixing is not prone to problems specific to mechanical mixing such as wear and expensive maintenance due to the presence of moving elements (e.g., impellers, shafts, ball bearings) inside the digester. Hence, there is a clear industrial interest in investigating gas mixing. Despite this, only [15, 14, 22, 23] have proposed robust multiphase models. [16] adopted a simplified approach by considering *de facto* a single-phase model and reproducing the effect of the bubbles through appropriate boundary conditions, but such approach is valid only for the specific case of the draft-tube digester they considered.

[15, 14, 22] used the Euler-Euler model for their simulations. It is well-known that the Euler-Euler model can handle very complex fluids, but needs a relevant quantity of empirical information to close the momentum equations, and for this reason [24] recommends it only when other models are not available. A novel Euler-Lagrangian CFD model introduced in [25] to simulate the gas mixing of sludge for anaerobic digestion is described in which fluid motion is driven by momentum transfer from the bubbles to the liquid. The bubbles rise in columns via buoyancy and transfer momentum to the surrounding sludge. This momentum transfer takes place due to the push force that the bubbles exert to the surrounding liquid, and the riptide effect arising from the low-pressure region created by the motion of the bubbles. This model successfully described a laboratory-scale setup with a much reduced amount of empirical information when compared to the Euler-Euler model. Validations were performed through Particle Image Velocimetry [25] and Positron Emission Particle Tracking [26] techniques.

Sludge is opaque, corrosive and biochemically hazardous: this makes experiments difficult to perform and therefore makes the use of CFD more valuable, but for the same reason it makes also the process of validation more difficult. The only experiments—and, consequently, validations—reported in the literature on full-scale anaerobic digesters consist of the introduction of a tracer fluid at the inlet and its detection at the outlet [17, 18]. They are costly experiments and only give a "black box" representation of the flow through the digester. Other approaches consist of comparing dimensionless groups calculated from specifications such as the power absorbed by the impeller [27, 28, 29]. [19, 20] reported the validation performed by [17], but did not perform any of their own. An alternative approach consists of providing a validation for a CFD model through laboratory-scale experiments, and then, applying the validated model to a set of full-scale scenarios. This approach has the advantage of informing modelling strategies involved in the full-scale simulations, such as bubble injection methods, boundary conditions or multiphase momentum transfers, and was followed in the work presented here.

Within this work, the model of [25] was applied to examine the mixing regime of a full-scale anaerobic digester. In gas-mixed digesters, biogas is taken from the top and pumped into the sludge at the base through a series of nozzles. The outcome of the simulations was analysed through a novel multi-facetted approach. First, velocity, shear rate and apparent viscosity flow patterns were considered, with the latter being examined for the first time. Then, the computational domain was divided into high, medium, low and very low shear rate zones and each zone's relative occupancy was reported, similar to how [12] considered the velocity magnitude. Finally, the concentration of a non-diffusive scalar tracer was studied. The flow patterns analysis reported for the first time the effect of non-Newtonian rheology on mixing; in particular, the issue of low-viscosity corridors was identified as a possible condition for detrimental, short-circuited mixing. The assessment of the shear rate relative occupancies showed that mixing is not significantly altered if mixing input power is lowered to a minimum acceptable level. The study of the tracer concentration made it possible to assess a mitigation strategy for the low-viscosity corridors. In practice, it was suggested to arrange a second series of concentric nozzles at a different radius from the tank centre, and to switch biogas injection between the original and the new series at regular time intervals.

2 CFD modelling

Sludge is a complex material, which displays a broad range of multiphase and rheological phenomena. In order to successfully model sludge within CFD work, it is necessary to introduce a series of assumptions and simplifications, depending on the type of sludge and the aims of the CFD study.

2.1 Multiphase Dynamics

Sludge is a mixture of water, biogas, flocculant and sedimenting debris, both organic and inert. The dimensions of the debris varies from molecules to sand and grit of approximately one millimetre. The dimension of the debris can increase to centimetres, if silage or food waste are added as in the case of agricultural digesters. In addition, gas mixing introduces an additional (gaseous) phase.

Given the level of complexity, some simplifying assumptions are necessary for modelling. Firstly, no information on scum or other floating matter is available from the industrial digesters used for the full-scale modelling work presented in this article, and therefore flocculation was ignored for the sake of simplicity. Sedimentation in the digesters is known to take place over a timeframe of years, while the retention times do not exceed one month. The problem of sedimentation within anaerobic digesters is important, complex and deserving of dedicated study. However, the focus of the work presented in this article is biogas yield optimization; hence, it is reasonable to ignore sedimentation. Finally, as wastewater is screened prior to primary sedimentation, it is reasonable to assume that larger debris is removed, and only fragments of the order of one millimetre are present in sewage sludge. As the computational mesh size was expected to be much larger and the trajectories of the single debris were of no interest in the analysis, it was natural to consider sludge as a single phase. The biogas bubbles constituted an obvious exception, as it was their motion that generated the sludge flow patterns.

2.2 Continuous Phase

Considering the foregoing discussion, it can be seen that the components of sludge (apart from the gas bubbles) can be approximated as a single, continuum phase. Given the predominance of water in the relative volume ratios, sludge was modelled as an incompressible, constant-density fluid obeying the Navier-Stokes equations.

2.3 Rheology of sewage sludge

Sludge is a complex material. Sludge characteristics depend on total solid content (TS) and temperature [30], and its rheology displays a broad variety of complex phenomena such as pseudoplasticity, viscoelasticity, shear banding and thixotropy [31]. Although a number of authors adopted the radical simplification of modelling sludge as a Newtonian fluid [15, 16, 17], pseudoplasticity has been reported to affect the flow patterns [32]. A simple, successful approach in anaerobic digestion CFD modelling has consisted of considering only the pseudoplastic behaviour while negletting all the remaining layers of complexity [14, 29, 12] This means that the (apparent) viscosity, instead of being constant, depends on the shear rate magnitude $|\dot{\gamma}|$ following a power-law relationship:

$$\mu = K\,|\dot{\gamma}|^{n-1} \ , \tag{1}$$

where K is the consistency coefficient ($\mathrm{Pa\,s}^n$) and n is the power law index. “Pseudoplastic” means $n < 1$. All the authors cited above used the experimental data of [33]. More recently, the Herschel-Bulkley model has been adopted [19, 20]. The Herschel-Bulkley is a power-law model, in which flow occurs only if the shear stress exceeds a critical value τ_0:

$$\mu = \tau_0\,|\dot{\gamma}|^{-1} + K\,|\dot{\gamma}|^{n-1} \ . \tag{2}$$

The authors cited above used the experimental data of [34] and, more recently, of [35] for digested sludge.

In the work presented here, the power-law model (Equation 1) was adopted following the data of [33] for TS values of 2.5, 5.4 and 7.5%. These values cover a wide range of sludge types used in industrial digesters—and in fact have already been investigated in previous literature [14, 29, 12]—and are similar to the conditions of the laboratory-scale validation of the present model [25]. In addition, the Herschel-Bulkley model (Equation 2) was also adopted following the data of [35] for 1.85% TS, and a Newtonian model was considered for comparison. Table 1 presents the details of these models. To avoid a singularity at $|\dot{\gamma}| = 0$, the numerical solvers adopt a Newtonian model continuously when the shear rate drops below a user-defined threshold. For the work reported in this article, this threshold was set to 0.001 s^{-1}. When appropriate, the curves reported in Table 1 were extrapolated beyond the experimentally-measured range. As in mesophilic conditions the temperature is kept constant at 35 °C, the temperature dependence can be dropped. As discussed in [25], the values of density for the TS range considered vary from 1,000.36 to 1,001.73 $\mathrm{kg\,m}^{-3}$ [30], which differ for

	TS (%)	τ_0 (Pa)	K (Pa s^n)	n (–)	$\lvert\dot{\gamma}\rvert$ range (s^{-1})
Power-law [33]	2.5	0	0.042	0.710	226–702
	5.4	0	0.192	0.562	50—702
	7.5	0	0.525	0.533	11—399
Herschel-Bulkley [35]	1.85	0.092	0.169	0.308	0.01–30
Newtonian	–	0	12	1	–

Table 1: Rheological properties of sludge. "$\lvert\dot{\gamma}\rvert$ range" refers to the limits of the shear range interval in which the experimental measurements were performed

less than 1% from water density at 35 degrees (994 $\mathrm{kg\,m^{-3}}$), and therefore density was approximated to 1,000 $\mathrm{kg\,m^{-3}}$ in all cases for simplicity.

2.4 Multiphase model

The Euler-Lagrange model for gas-mixing in anaerobic digestion developed and validated with lab-scale data in [25, 26] was adopted for the work presented within this article.

Mixing is driven by diffusion, turbulent diffusion and advection [36]. While the first is related to the biochemical properties of sludge, the latter two pertain to physical modes of mixing, and hence the discussion focusses on them. In an unconfined, gas-mixed digester, turbulent diffusion occurs due to the swift motion of the rising bubbles, and is confined to the immediate proximity of the bubbles. However, in a full-scale plant, the bubbles are arranged in vertical plumes the diameter of which is small compared with the digester size, and therefore such a mechanism becomes negligible. Hence, advection was considered as the main mixing mechanism. Thus, the aim of the multiphase model is to reproduce the flow patterns away from the bubble plume, without necessarily resolving the bubble motion in detail on the basis that, in a full-scale plant, turbulent diffusion around the bubble plume is negligible, and therefore the details of the liquid phase motion near the bubbles are not of interest [25]. For this reason, the following approximations were made: (*i*) spherical bubbles, (*ii*) pointwise bubbles, and (*iii*) no bubble-bubble interaction. In parallel with these assumptions, a two-way coupling was defined such that sludge exchanges momentum with single parcels (biogas bubbles), and the force acting on the single bubbles is broken down into buoyancy, drag and lift forces. Bubble drag and lift forces were reproduced with the models developed by Dewsbury et al. [37] and Tomiyama et al. [38] respectively. As explained in [25], the drag force depended on the particle Reynolds number, which in turn was computed from the sum of the eddy and apparent viscosity.

Nominal bubble diameter is requested by the model as an input to compute the force acting on each bubble. However, there are no data in the literature about the dimension of the bubbles inside a digester—this is unsurprising, as the problem of measuring bubble size inside an industrial digester presents the same afore-mentioned challenges of determining full-scale digester flow patterns experimentally. In addition, bubbles are expected to expand when rising. Under these circumstances, the approach followed in this work was to run multiple series of simulations, each with a fixed bubble size. In this way, albeit the outcome of a single run may depend on the particular choice of a given bubble size, common trends can be identified and used to give predictions that hold for all the different choices of bubble size. For the work presented within this article, the values of d = 2, 6 and 10 cm were chosen.

2.5 Meshing

In this article, a CFD simulation consisting of a series of transient PISO runs is described. The modelled digester comprises a cylindrical digester with an inclined base (Figure 1) (i.e., a cylinder over an inverted cone) with twelve nozzles placed along a circle at the bottom of the tank. Details of the digester are reported in Table 2.

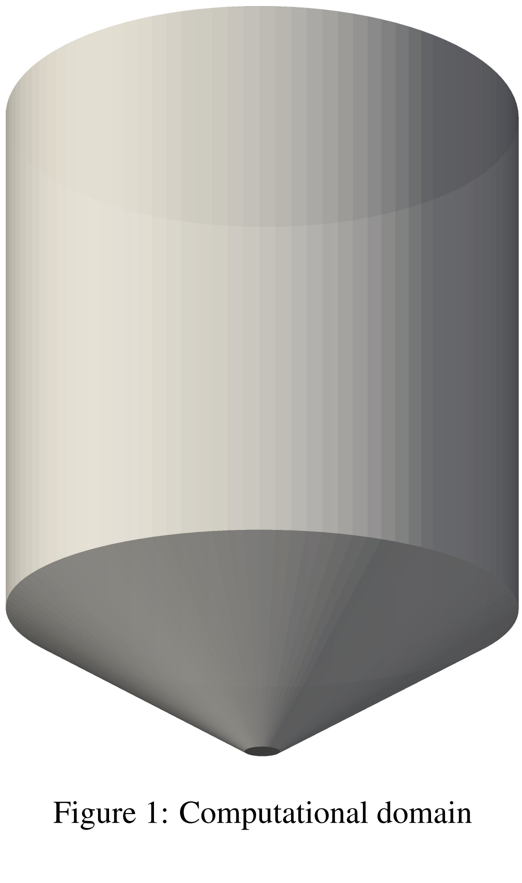

Figure 1: Computational domain

The model domain consists of a wedge comprising an angle of $\pi/6$ radians. A single nozzle lies on the symmetry plane of the wedge. Four grids were generated—the details are reported in Table 3. As an example, Figure 2shows side elevation, plain view and two details of Grid 2.

The computational work was undertaken using the BlueBEAR high performance computing facility at the University of Birmingham. Each simulation was run in parallel on three dual-processor 8-core 64-bit 2.2 GHz Intel Sandy Bridge E5-2660 worker nodes with 32 GB of memory, for a total of 48 nodes. OpenFOAM 2.3.0 was used to run the computational work.

In [25] the Reynolds stress Launder-Gibson model [39] was successfully employed

External diameter	D_{ext}	14.63 m
Diameter at the bottom of the frustum	D_{int}	1.09 m
Cylinder height	h	14 m
Frustum height	h_0	3.94 m
Distance of the nozzle from the axis	R_{noz}	1.75 m
Distance of the nozzle from the bottom	h_{noz}	0.3 m
Maximum gas flow rate per nozzle	$Q_{\max}$	$4.717\ 10^{-3}\ \mathrm{m}^3\mathrm{s}^{-1}$

Table 2: Details of the digester geometry (courtesy of Peter Vale and Severn Trent Water Inc.)

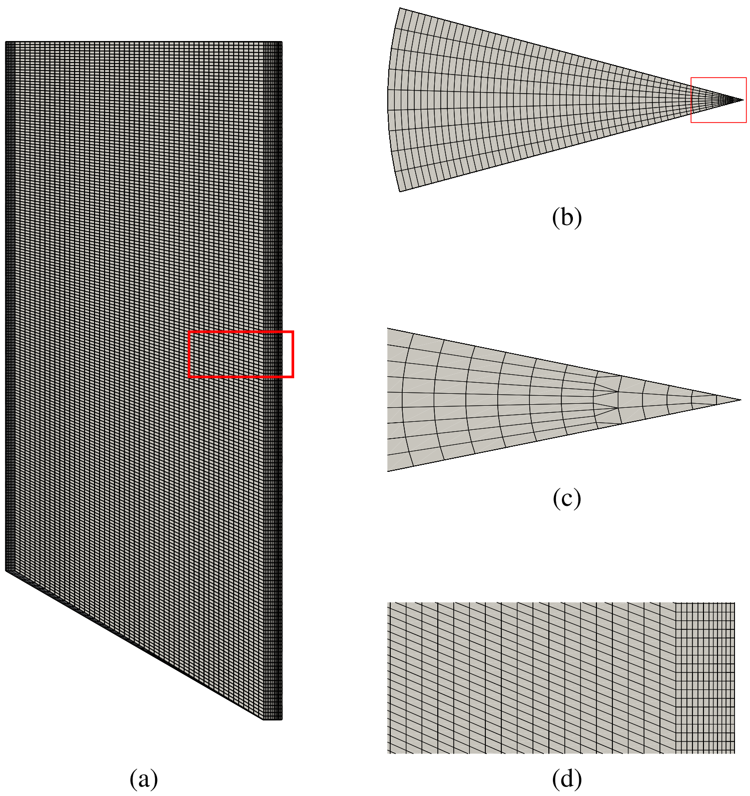

Figure 2: Grid example. Side elevation (a) and plain view (b), wedge apex (c) and side detail (d). The areas occupied by (c) and (d) are identified in (b) and (a) respectively

Id.	Number of cells	Max skewness	Max aspect ratio	Non-ortho max	Non-ortho avg	Volume min (m^3)	Volume max (m^3)	Vol wedge (m^3)
1	394,400	1.123	13.24	30.03	14.00	1.500e-5	1.011e-3	215.8
2	98,420	1.064	9.974	30.00	13.66	3.158e-5	4.241e-3	215.8
3	36,720	1.112	10.53	30.03	13.78	3.333e-5	1.116e-2	215.3
4	18,760	1.304	13.54	30.01	13.84	4.286e-5	2.144e-2	215.3

Table 3: Details of the grids

to reproduce the turbulent motion of the liquid around the bubbles and therefore the same model was employed in the study reported here. The timestep was defined dynamically with an algorithm aimed at keeping the maximum Courant number just below a specified value of 0.2, in the same way as in [25]. For a given cell i of linear magnitude L_i where the fluid velocity is $|\mathbf{u}_i|$, given the timestep Δt, the Courant number is defined as:

$$\mathrm{Co}_i = \frac{|\mathbf{u}_i|\ \Delta t}{L_i}\ . \tag{3}$$

The maximum Courant number, Co, is the maximum value of Co_i over i. Following [25], after a small initial value of 10^{-5} s, the timestep was corrected to keep the maximum Courant number near but less than the limit of 0.2. At each timestep, the solution was considered as converged when the residual for the pressure fell below 10^{-7}, and all the other quantities below 10^{-6}.

The initial condition for the fields simulated within the numerical work presented here consists of a system configuration in which the bubble plume is fully developed. In [25] this condition was obtained by performing a series of preliminary, first-order (transient) runs in which the bubble column developed from a state in which there were neither bubbles nor liquid phase motion. In the work described here, preliminary runs were performed for a computational time of 60 s. Then the last timestep was used as initial condition for a series of main (second-order) runs while the previous timesteps were discarded. The second-order runs were performed for an additional 240 s, for an overall computational time of 300 s. As in [25], binary files were collected for every integer-second timestep of the main runs.

The boundary conditions are reported in Table 4. The values of C_μ, κ and E for the wall functions were set to 0.09, 0.41 and 9.8 respectively. The initial conditions for the preliminary runs were: 4.95 $10^{-4}\ \mathrm{m}^2\,\mathrm{s}^{-3}$ for the ε field, zero for p, u and R_{ij}. The differencing schemes used were: linear for interpolations, limited central differencing for the Gradient operator, linear for the Laplacian, Van Leer for all the other spatial operators, first-order Eulerian scheme for the time derivative in the preliminary runs and second-order backward for the main runs.

The computational runtime remained below 20 hours per run, and the timestep was observed to be between 0.0013 and 0.14 seconds.

2.6 Mesh size dependency analysis

In an Euler-Lagrangian model, the parcels (in our case, single bubbles) are approximated to be pointwise, and therefore the mesh size should be much larger than the parcel diameter in order to respect this approximation [40]. In [41, 42] it was shown that this requirement can be relaxed to the point of having a mesh volume comparable with parcel volume under certain conditions (number of parcels below $\sim 10^3$), but nevertheless care must be taken in order to avoid resolving the hydrodynamics of the fluid around the bubble when the mesh cell size is similar to the bubble diameter and, hence, mesh-dependant results when the mesh size becomes smaller than the parcel size [25]. This is possible, as the bubble volumes are $4 \cdot 10^{-6}$, 10^{-4} and $5 \cdot 10^{-4}$ m^3 for diameters of 2, 6 and 10 cm respectively, which means that bubble sizes are between 0.3 and 40 times the smallest cell size in Grid 1, and between 0.004 and 4 times the largest cell in Grid 1. A grid independence test is always appropriate in research involving CFD simulations in order to identify a mesh that is refined enough to secure mesh-independent results. In addition, with the specific model adopted in this work, it was shown in [25] that such a test is necessary to exclude meshes that are too fine compared to the bubble size.

For the reasons cited above, the Grid Convergence Index (GCI) proposed by [2] was performed and a series of mesh independence tests was run. Two tests were performed for each run series, one involving Grids 1, 2 and 3, and another one involving Grids 2, 3 and 4. The tests were performed over all the values for TS and d and $q = 1$, the latter being justified by the fact that the number of bubbles in the computational domain is greater for higher flow rates. All the details of the mesh independence test are similar to the procedure detailed in [25]; the only difference being that the volume proportion of the shear rate interval $\langle \dot{\gamma} \rangle \in [0, 0.1]$ s^{-1} was considered in place of the average shear rate. This was because the proportions of different shear rate intervals were used in the discussion to assess mixing quality, as will be shown in Section 3.3.

Top	p	Pressure	Constant zero
	$\mathbf{u}$	Velocity	Slip
	ε	Turb. dissipation	Slip
	R_{ij}	Reynolds stress	Slip
Wall/bottom	p	Pressure	Adjusted such that the velocity flux is zero
	$\mathbf{u}$	Velocity	Constant zero
	ε	Turb. dissipation	Standard wall function
	R_{ij}	Reynolds stress	Standard wall function
Front/back	All		Cyclic

Table 4: Boundary conditions [25]

3 Discussion

A series of runs was performed for values of gas flow rate corresponding to fractions of $Q_{\max}$ viz. $q \equiv Q/Q_{\max}$ = 0.1, 0.2, 0.3, 0.5, 0.7 and 1.0.

3.1 Assessment of the mesh dependence

The results of the GCI study are reported in Table 5. For each run, two tests were performed, one involving Grids 1, 2 and 3, and one involving Grids 2, 3 and 4. The grids of a given test were considered to be in the asymptotic range of convergence when the asymptotic convergence indicator differed from the value of 1 by less than 25%. In such cases, the value of the indicator is shown in Table 5. The test was performed for all values of TS and d to assess the effect of these variables on grid convergence.

For almost all the combinations of TS and d values, either all the grids were in the asymptotic range of convergence (both Asymp.1 and Asymp.2 are evidenced), or Grids 1, 2 and 3 were in the asymptotic range of convergence but not Grids 2, 3 and 4 (Asymp.1 is evidenced but not Asymp.2), or the converse (Asymp.2 is evidenced but not Asymp.1). In the second case, Grid 4 was too coarse to be within the mesh-independence range; in the third case, the cells composing Grid 1 were as small as, or smaller than, the individual bubbles and the simulation results became mesh-dependent. In all the cases, Grid 2 was within the asymptotic range of convergence. For this reason, Grid 2 was used for further simulations.

3.2 Flow patterns

Figures 3, 4 and 5 show the velocity field at the last timestep (300 s)). The inlet position is marked with a white triangle. All values of TS (%), bubble diameter (d), and air flow rate (q = 1, 0.5, 0.2) are shown. It can be observed that the general structure of the flow patterns is the same for all runs. The rise of the bubbles forms a column of fast rising liquid phase above the nozzle. Once it reaches the surface, the liquid phase is displaced horizontally towards the exterior, and then forms a large vortex that occupies most of the remaining part of the domain. The centre of the vortex is located approximately at the centre of the upper part of the domain. Once inside the vortex, the liquid phase slowly descends along the external boundary of the domain, follows the slope of the bottom of the tank and finally approaches the zone around the nozzle. Advection throughout the whole digester is the driving mixing mechanism, as discussed in Section 2.4.

Beyond this general description, effects arising as a result of the gas flow rate, the rheology (as a function of TS) and the bubble size can be observed. Specifically, the velocity magnitude increases and the vortex becomes more and more developed as gas flow rate, q rises; in particular, the vortex does not reach the lower part of the domain for small values of q. The vortex becomes less compact and the velocity patterns are

Table 5: GCI analysis

	2.5% TS			5.4% TS			7.5% TS		
	$d = 2$ cm	$d = 6$ cm	$d = 10$ cm	$d = 2$ cm	$d = 6$ cm	$d = 10$ cm	$d = 2$ cm	$d = 6$ cm	$d = 10$ cm
SpVol_4	0.53	0.5	0.6	0.59	0.530	0.6	0.6	0.5719	0.6
SpVol_3	0.57	0.6	0.47	0.553	0.57990	0.6	0.6	0.625100	0.5
SpVol_2	0.544	0.5	0.51	0.543	0.5780	0.5	0.6	0.62540	0.63
SpVol_1	0.5469	0.7	0.6	0.60	0.702	0.6	0.6	0.5624	0.670
p_2	1.463	0.710	3.787	5.948	14.32	1.220	1.070	24.31	1.047
p_1	6.343	0.790	1.237	3.189	7.060	—	0.594	9.440	4.355
$\mathrm{GCI2}_{43}$	0.18	1.3	0.2	0.03	0.005	0.3	0.4	5e-4	0.8
$\mathrm{GCI2}_{32}$	0.08	0.8	0.04	0.004	4e-5	0.3	0.2	1.6e-7	0.6
$\mathrm{GCI1}_{32}$	0.007	0.7	0.19	0.013	5e-4	—	0.4	2e-5	0.08
$\mathrm{GCI1}_{21}$	3e-4	0.6	0.3	0.04	0.009	—	0.3	0.0018	0.010
Asymp.2	1.40	**1.24**	1.50	**0.98**	**1.06**	0.59	1.37	**1.00**	**0.92**
Asymp.1	**1.16**	**0.86**	0.39	0.076	0.0020	—	**0.88**	1.5e-4	**1.06**

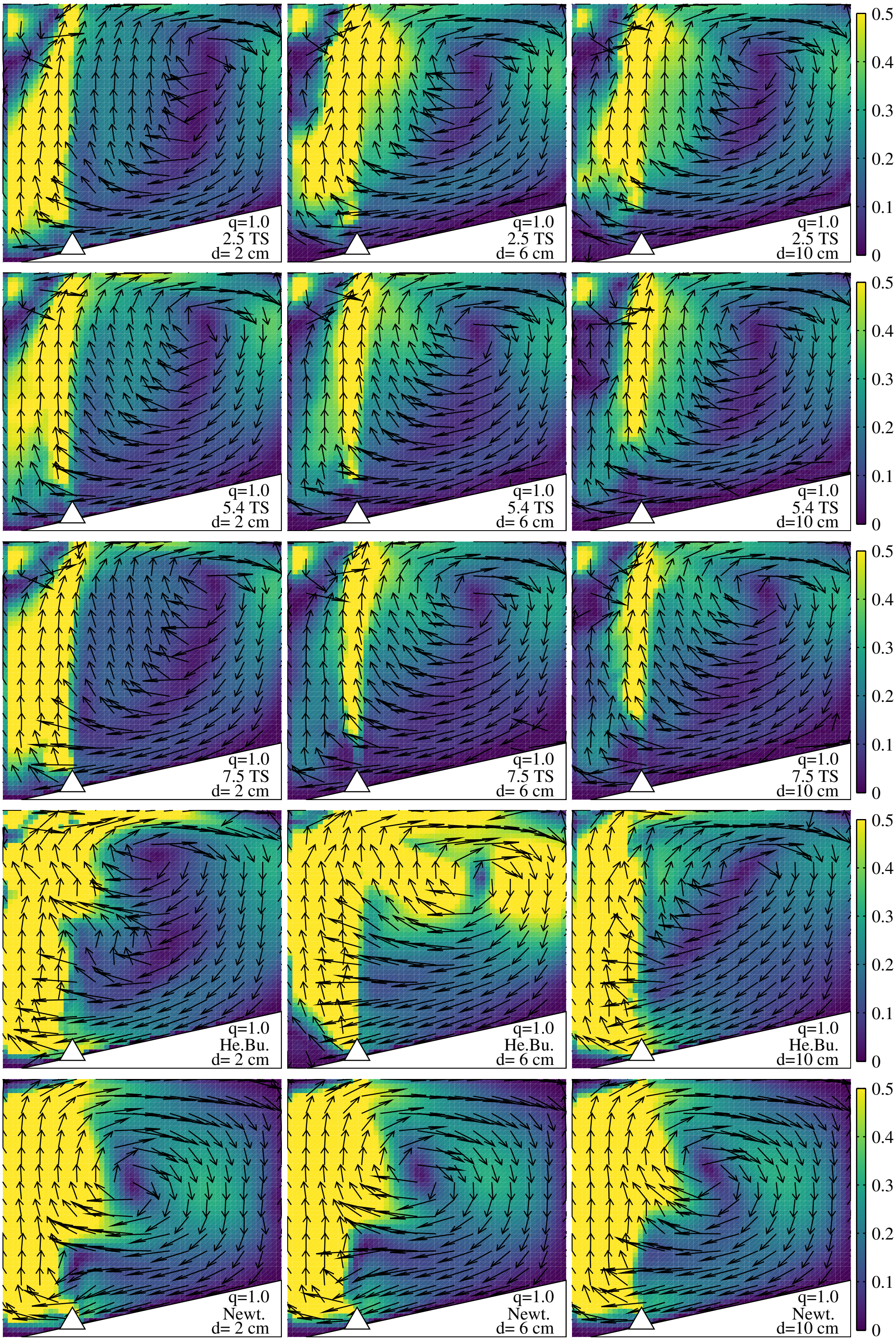

Figure 3: Flow patterns for $q = 1.0$ with $|\mathbf{u}| \in (0\,, 0.5)\ \mathrm{m\,s^{-1}}$

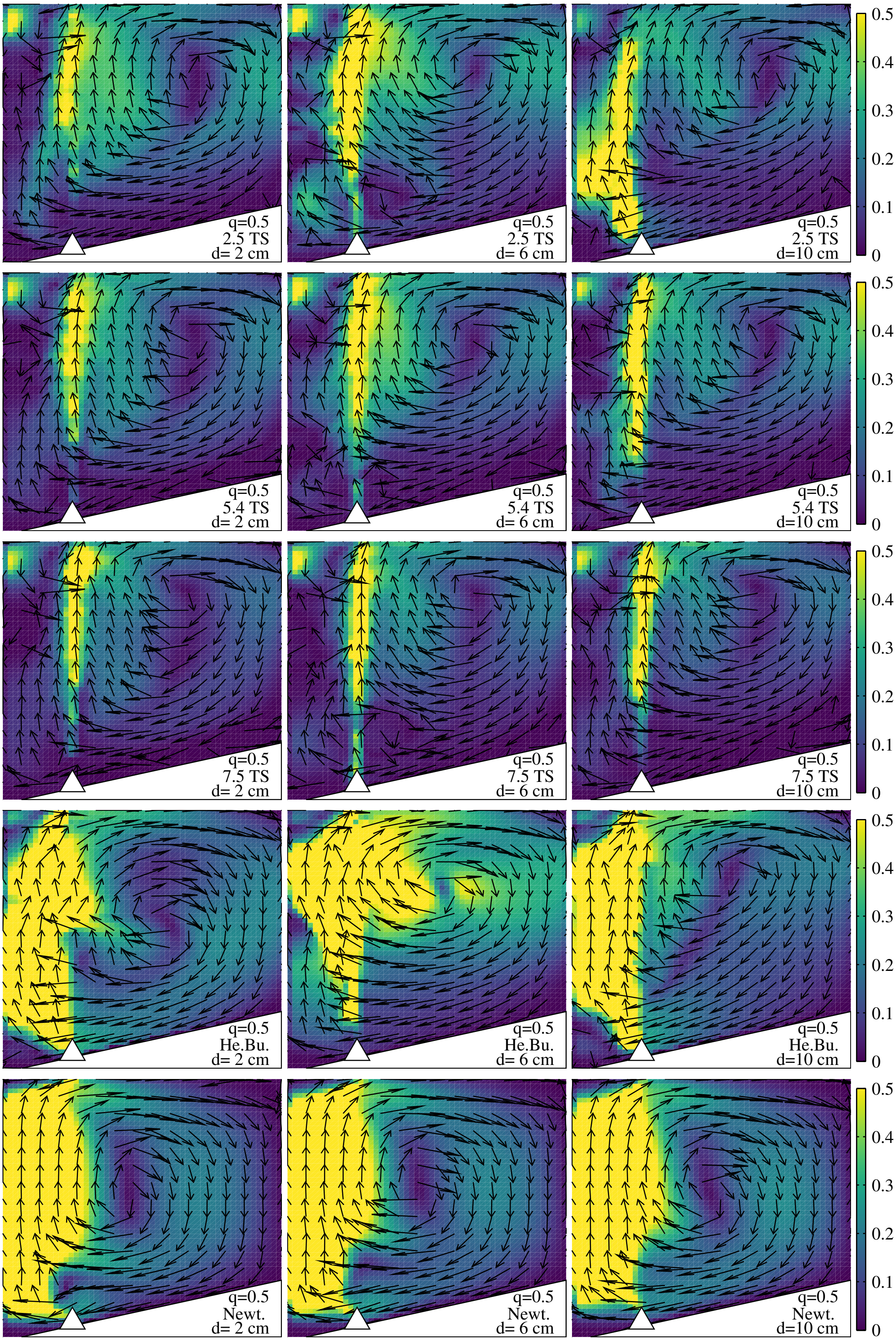

Figure 4: Flow patterns for $q = 0.5$ with $|\mathbf{u}| \in (0\,, 0.5)\ \mathrm{m\,s^{-1}}$

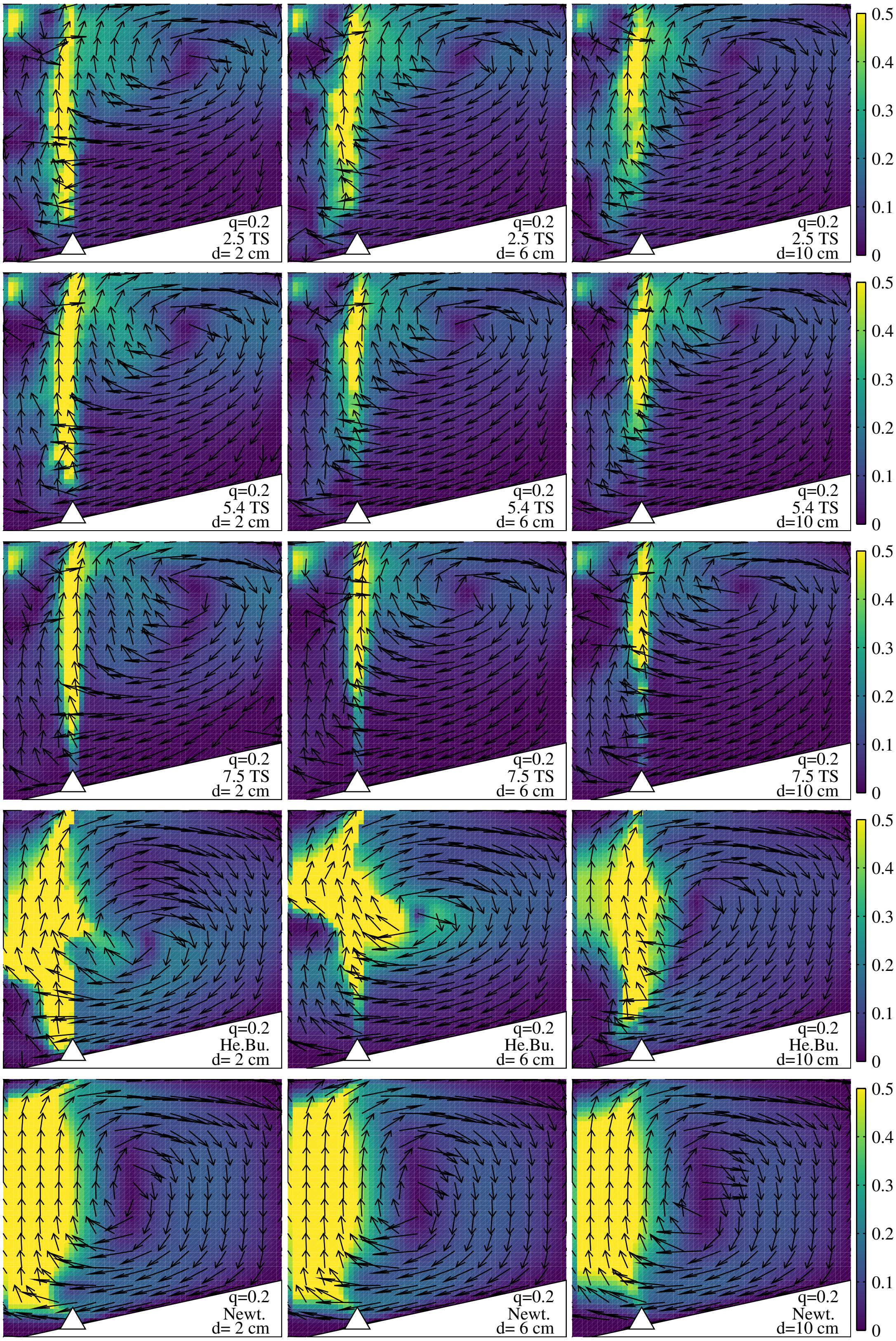

Figure 5: Flow patterns for $q = 0.2$ with $|\mathbf{u}| \in (0\,, 0.5)\ \mathrm{m\,s^{-1}}$

more dispersed as TS rises—on the other side, an increase of gas flow rate brings to the creation of more bubbles, and hence momentum transfer is increased and the main vortex is developed more widely. Finally, the shape of the vortex changes slightly; i.e., the vortex is more extended when d is small.

An analysis of viscosity under different flow regimes was undertaken. Figures 6, 7 and 8 depict the viscosity field at the last timestep for all the values of TS and d (q = 1, 0.5 and 0.2). It can be seen that the viscosity drops along the vertical column and, more interestingly, along the descending branch of the vortex. This is due to the fact that sludge is a pseudoplastic fluid, and its viscosity decreases when shear rate increases. As a consequence of this, flow patterns in which the viscosity is considerably lower than in the surroundings arise inside the domain. Such patterns can be observed in Figure 6 as the rising column and the vortex descending branch.

The low-viscosity domains offer less resistance against incoming liquid, when compared to surrounding high-viscosity zones. Hence, it is reasonable to expect that circulation will be enhanced within the low-viscosity areas and, conversely, will be inhibited in the surrounding high-viscosity zones. This is expected to have a detrimental effect in the uniform distribution of nutrients throughout the digester, and therefore is not desirable.

3.3 Average shear rate

Following the seminal work presented in [43], average shear rate has become a fundamental process characteristic to classify mixing in vessels in the water industry [12]. Despite the fact that the representation of complex flow patterns with one number is something of a simplification, [44], the concept of average velocity gradient is still useful in environmental engineering design [45].

[12] reported an analysis of an impeller-stirred lab-scale digester with different TS values and rotational regimes. In that work, high, medium and low-velocity zones were identified, and additionally, the average shear rate was computed. The conclusions of [12] can be summarized as: *(i)* an increase of TS raises the volume of low-mixed zones, but does not have significant effects on the volume of the high-mixed zones; *(ii)* a change of the impeller angular velocity scarcely affects the average shear rate in the bulk of the domain; *(iii)* in all cases considered, the average shear rate was well below (up to an order of magnitude) of the suggested value of 50—80 s^{-1} [45] for optimum mixing, and yet biogas production was achieved.

The considerations above show that, for an impeller-stirred lab-scale digester such as the one reported in [12], mixing power input of an anaerobic digester can be lowered without affecting the average shear rate significantly. It is hypothesised here that these conclusions can be extended to a gas-mixed, full-scale digester. In order to verify this statement, the average shear rate $\langle\dot{\gamma}\rangle$ was plotted against q for different TS and bubble diameters and the results are shown in Figure 9. It can be seen that the behaviour of average shear rate depends on both TS and bubble size. For instance, for a bubble diameter of 2 cm $\langle\dot{\gamma}\rangle$ grows proportionally to q, but the rate of increase slows slightly

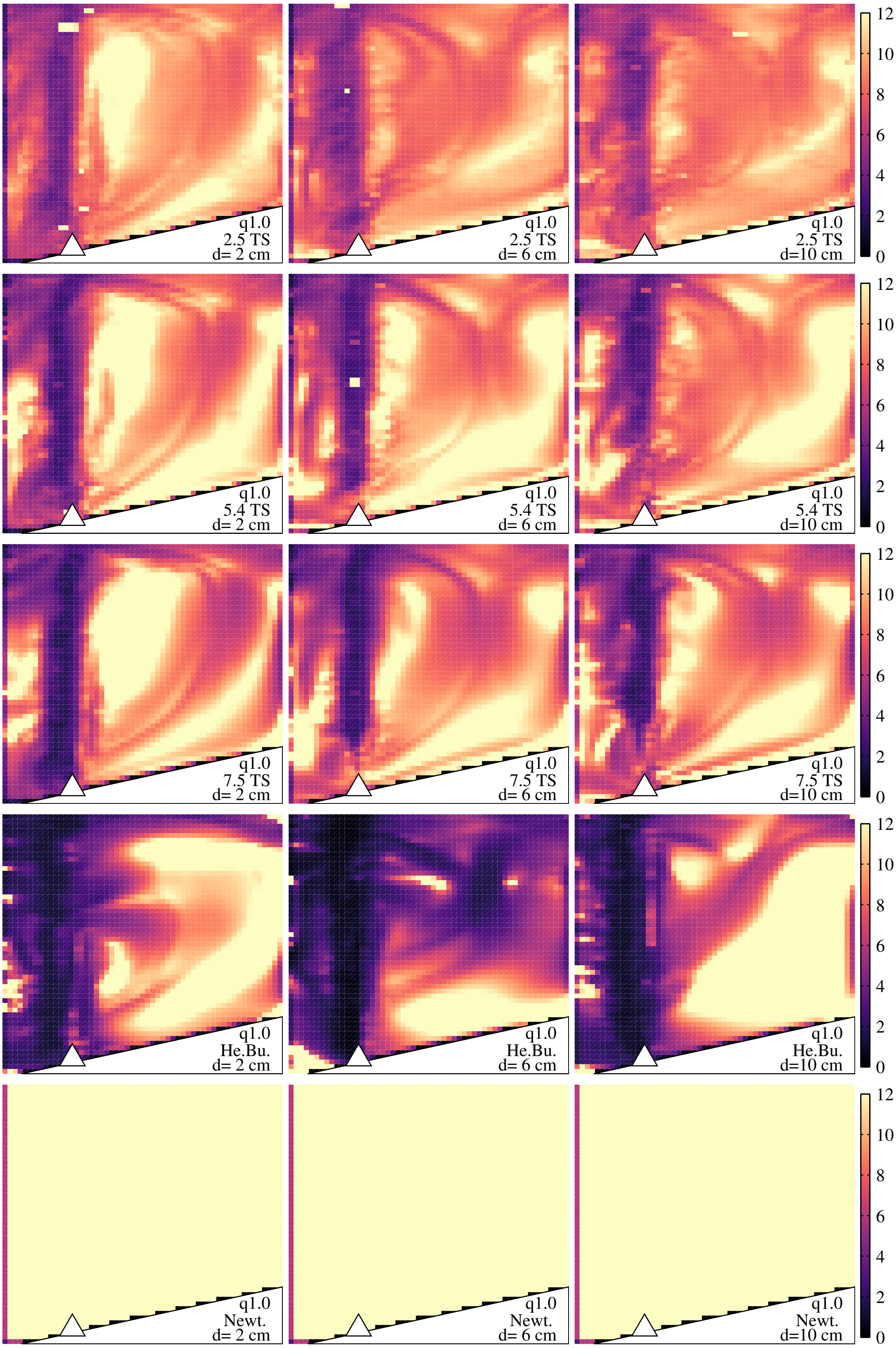

Figure 6: Apparent viscosity for $q = 1.0$ with $\mu \in (0\,,0.1)$ Pa s for the 2.5 TS runs, $(0\,,0.6)$ Pa s for the 5.4 TS runs, $(0\,,2.0)$ Pa s for the 7.5 TS runs

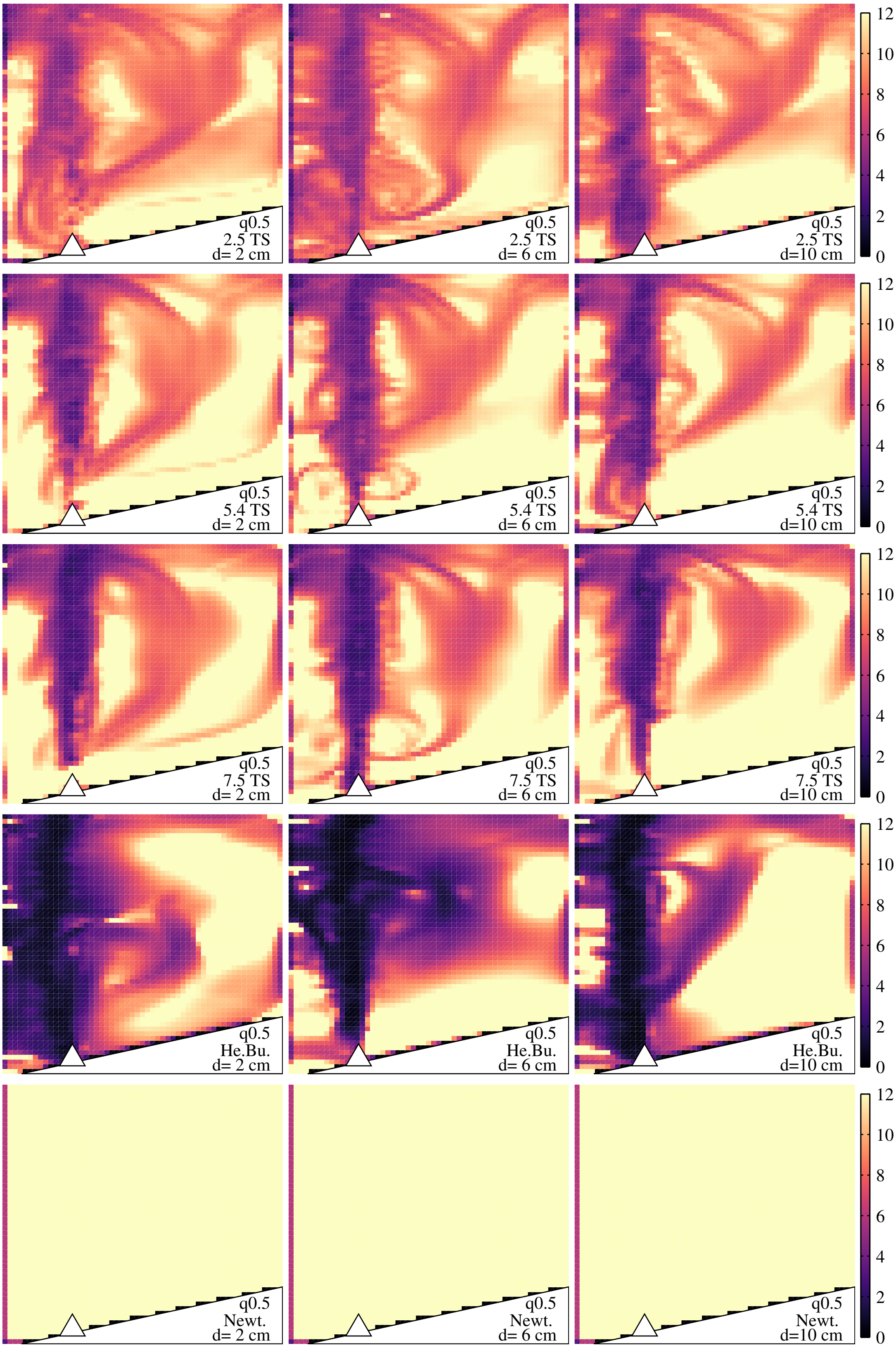

Figure 7: Apparent viscosity for $q = 0.5$ with $\mu \in (0\,, 0.1)$ Pa s for the 2.5 TS runs, $(0\,, 0.6)$ Pa s for the 5.4 TS runs, $(0\,, 2.0)$ Pa s for the 7.5 TS runs

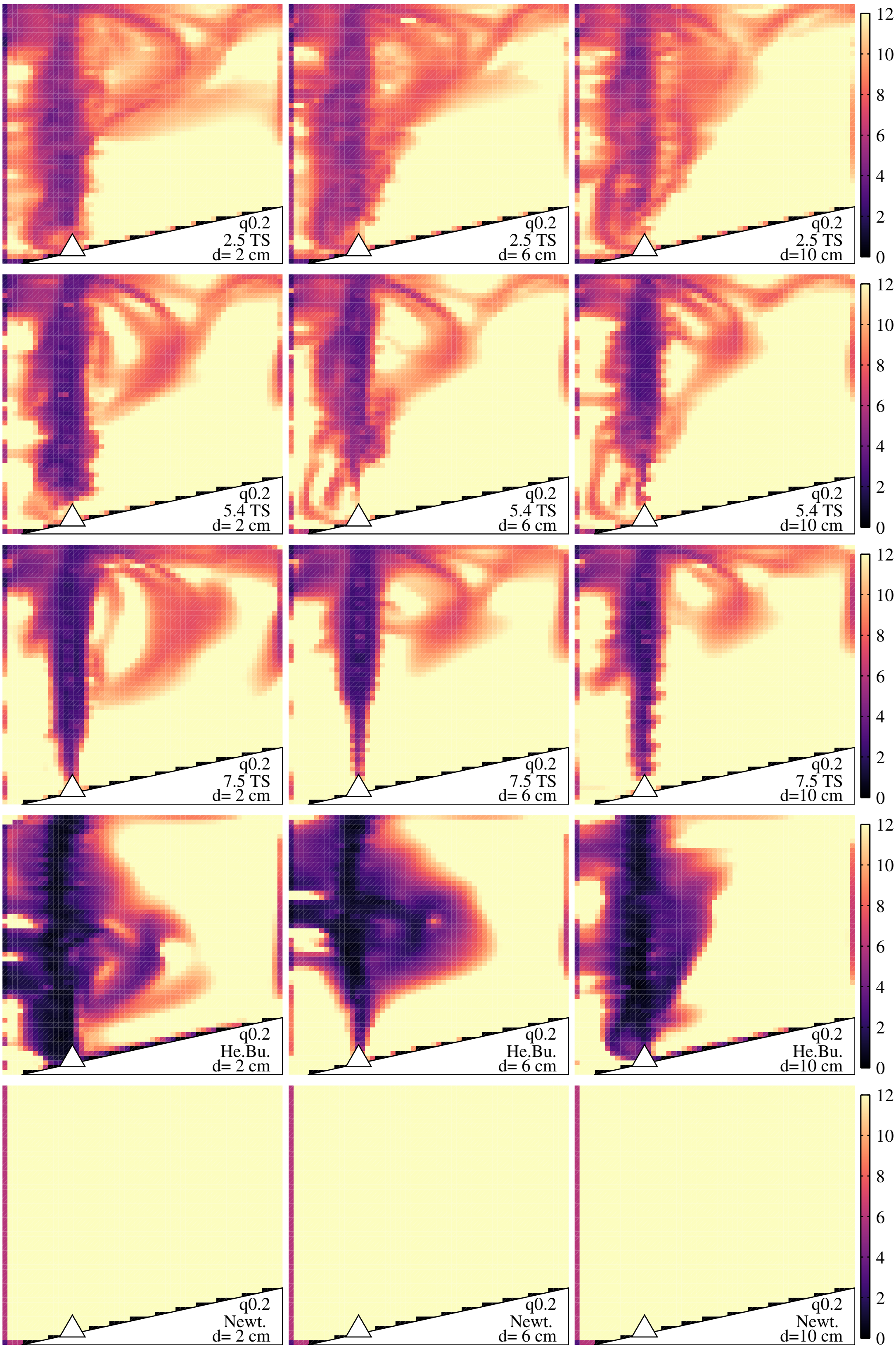

Figure 8: Apparent viscosity for $q = 0.2$ with $\mu \in (0\,, 0.1)$ Pa s for the 2.5 TS runs, $(0\,, 0.6)$ Pa s for the 5.4 TS runs, $(0\,, 2.0)$ Pa s for the 7.5 TS runs

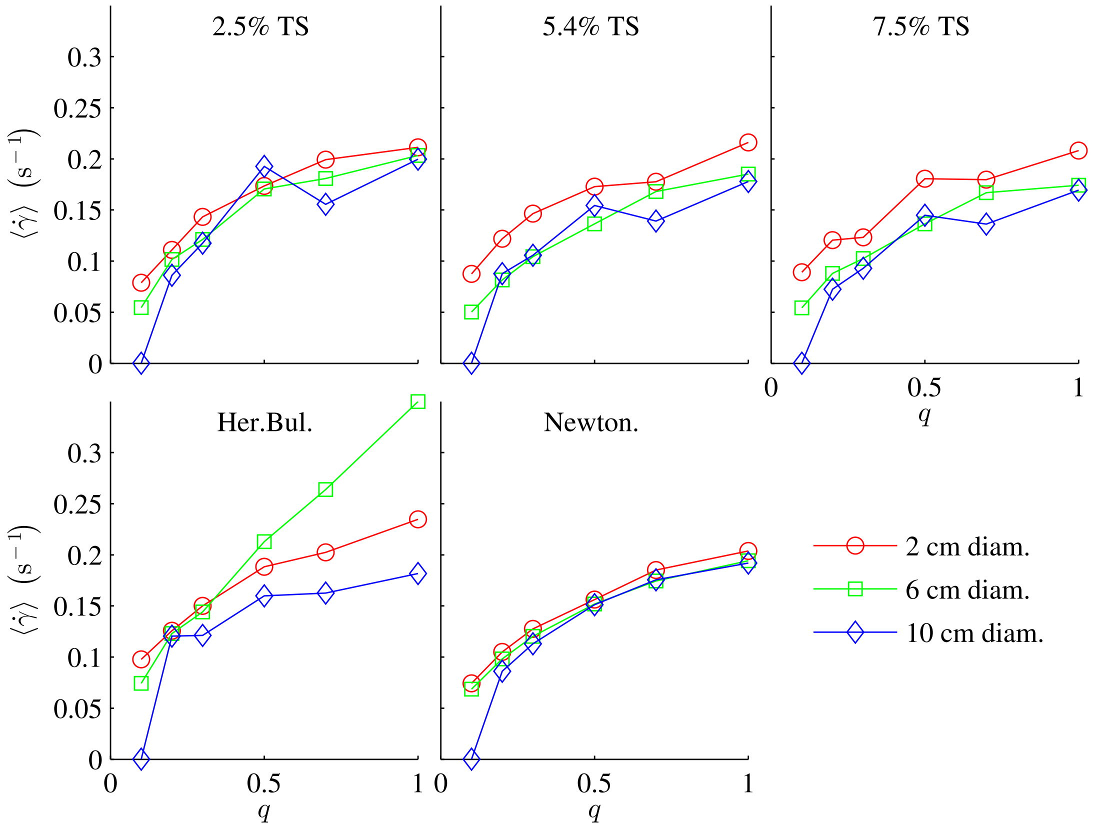

Figure 9: Average shear rate against the power input for different values of TS and d

for $q \geq 0.25$ and, more pronouncedly, for $q \geq 0.7$. This behaviour is reproduced by the 6 cm and 10 cm bubble size runs, with the difference that the decrease happens for values of q between 0.5 and 0.7, but not for 7.5% TS, where the decrease is not achieved. Apart from these differences, however, the relevant points that Figure 9 shows are: *(i)* the trend generally shows a similar growth for all the TS and bubble diameters, with a slower growth at $q \geq 0.7$, with similar values of $\langle\dot{\gamma}\rangle$ for all the runs; *(ii)* in all the cases and, relevantly, in the case $q = 1$ which is known to correspond to real, well-working digesters, the average shear rate is lower than the values suggested by widely-accepted literature [45] for optimum mixing, proving that such a criterion should not be applied to the case of gas mixing in full-scale anaerobic digestion.

An analysis was also undertaken on the proportions of different shear rate intervals. Four shear rate intervals were defined: $\langle\dot{\gamma}\rangle < 0.01$ s^{-1} (very low), $0.01 \leq \langle\dot{\gamma}\rangle < 0.1$ s^{-1} (low), $0.1 \leq \langle\dot{\gamma}\rangle < 1$ s^{-1} (medium), $\langle\dot{\gamma}\rangle > 1$ s^{-1} (high). The results are shown in Figure 10. The magnitude and behaviour of the shear rate relative volumes are similar for all the TS irrespective of bubble diameter. In particular: *(i)* the relative vessel volume with very low shear rate is initially high (approximately 0.5), then drops quickly to assume low values at $q = 0.3$—0.7; *(ii)* low shear rate relative volume is roughly constant with a value of approximately 0.5; *(iii)* the medium shear rate relative volume

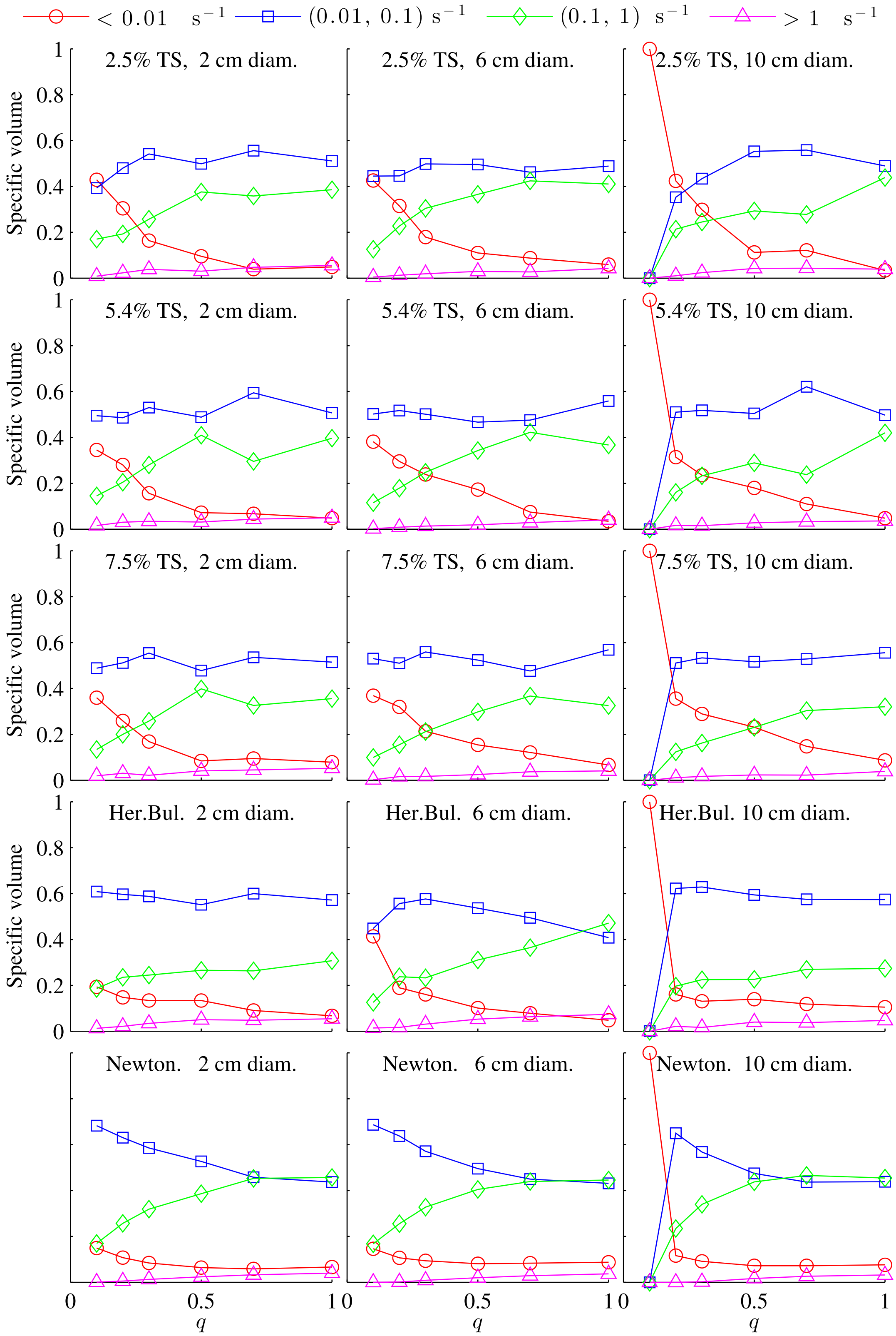

Figure 10: Specific volume of the shear rate intervals against flow rate for different values of TS and d

shows a growing trend up to $q = 0.5$—0.7 and then is approximately constant; *(iv)* the high shear rate relative volume is always negligible, but increases proportionally with q; *(v)* most of the volume is occupied by very low shear rate up to $q \simeq 0.2$; very low, low and average shear rates equally occupy the domain for q from 0.2 to 0.5—0.7; and for q greater than 0.5—0.7 most of the volume is equally occupied by low and average shear rates.

As the high shear rate relative volume is negligible, the effectiveness of mixing is expected to depend on the mutual balance of very low, low and average shear rate relative volume, rather than on an absolute criterion such as the one proposed by [45]. In particular, good quality mixing can be defined as when the average shear relative volume is high compared to the relative occupancies of the other shear rate intervals, and, similarly, very low shear relative volume is low. Considering the results shown in Figure 10, this condition can be considered to be verified for $q \geq 0.5$.

The power input for a single nozzle is [14]:

$$E = P_1 Q \ln\left(P_2/P_1\right) \ , \tag{4}$$

where Q is the volumetric flow rate, P_1 is the absolute pressure at the surface (that is, the atmospheric pressure), and P_2 is the absolute pressure at the nozzle (that is, $P_2 = P_1 + \rho g H$ if the nozzle discharges at the same pressure of the surrounding fluid, as in the case presented here). Considering the value of Q_{max} in Table 2, the value of the total power per volume unit corresponding to $q = 0.5$ is 1.079 $\mathrm{W\,m^{-3}}$, which can be effectively approximated to 1 $\mathrm{W\,m^{-3}}$. This value corresponds to half of the mixing power for $q = 1$ of 2.159 $\mathrm{W\,m^{-3}}$, and is significantly lower than the input mixing power of 5—8 $\mathrm{W\,m^{-3}}$ recommended by US EPA for proper mixing [46]

3.4 Switching nozzles

An alternative way to improve mixing by amending the geometry of the digester—specifically, by arranging a second concentric series of nozzles at a different distance from the tank symmetry axis was modelled. Biogas injection was switched between the original and the new nozzles series, at constant time intervals. This strategy differs from, and is complementary to, what literature commonly defines as alternated mixing. "Alternated" mixing means that the mixing mechanism (which is in principle not limited to gas mixing) is activated only for given time intervals as opposed to continuous mixing, where mixing is always active. As such, the strategy of switching nozzles can be applied to continuous and alternated mixing. In order to avoid confusion, "alternated" here refers to the mode of mixing consisting of activating and de-activating the mixing mechanism at given time interval, while "switched" or "switching" refers to the mixing strategy consisting of changing biogas injection between two nozzle series.

The effectiveness of the switching nozzles strategy was tested by performing a series of simulations, with the additional nozzle series being placed at a distance $R'_{\mathrm{noz}} = 5.49$ m from the tank axis. The value of $q = 0.5$ was chosen, in line with

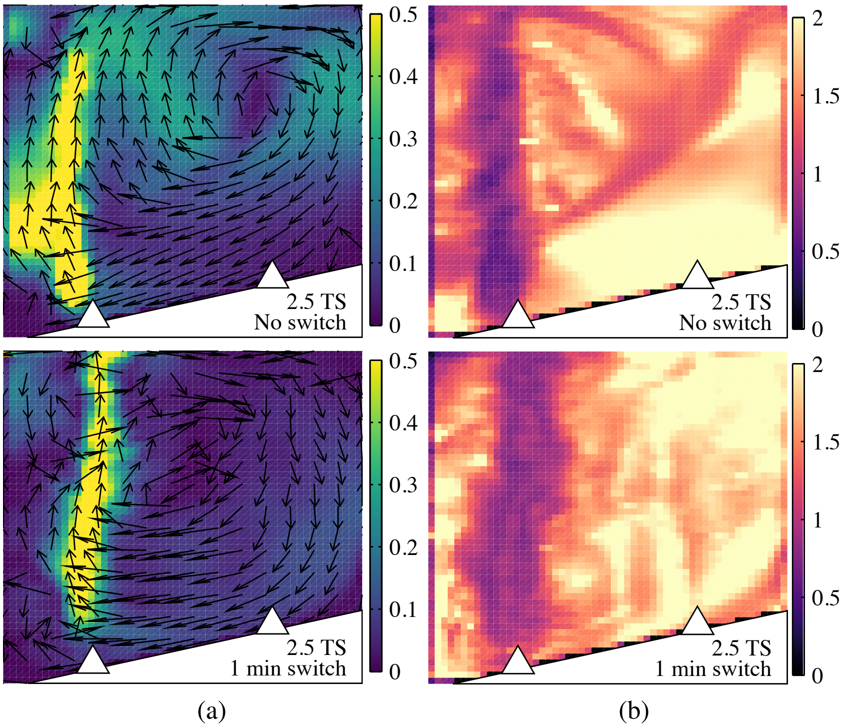

Figure 11: Comparison between original nozzle setup and one-minute switching for $q = 0.5$ and 2.5% TS. (a): Flow patterns with $|\mathbf{u}| \in (0\,, 0.5)\ \mathrm{m\,s^{-1}}$. (b): Viscosity with $\mu \in (0\,, 0.1)$ Pa s.

the conclusions on minimum mixing power per volume unit outlined in Section 3.3. In Section 3.3 it was shown that the outcome of the simulations does not depend on bubble size; however, the computational expense is proportional to the number of bubbles inside the system. For these reasons, $d = 10$ cm was chosen as the bubble size for all the simulations. During the simulations, biogas injection was switched every minute, for a total period of 5 minutes.

The results of the simulations are shown in Figure 11. The low-viscosity corridor corresponding to the descending vortex branch is absent under the switching-nozzles strategy. However, such rapid switching leads to a significant attenuation of the flow patterns; the velocity magnitude becoming substantially lower everywhere apart from the immediate vicinity of the bubble plume. This can be attributed to the fact that the system needs a non-zero time in order to develop flow patterns as the ones described in Section 3.2. The time interval of one minute is evidently too short for the system to develop significant flow patterns away from the bubble plume. It is not clear whether this situation corresponds to a better or worse level of mixing, and hence, a further investigations was undertaken.

A second analysis was performed by defining a non-diffusive tracer the concentra-

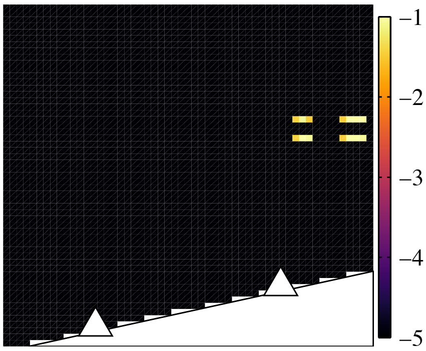

Figure 12: $\log_{10} \chi$ at the initial timestep. $\chi = 1$ inside the small quares, 0 elsewhere.

tion of which obeys the following equation:

$$\partial_t \chi + (\mathbf{u} \cdot \nabla) \chi = 0 \; . \tag{5}$$

At $t = 0$, a maximum tracer concentration was defined in four locations inside the domain, as shown in Figure 12.

Figure 13 shows the distribution of χ after 20 minutes, in the original (non-switched) nozzles configuration, and in setups where biogas injection was switched every minute and every five minutes respectively. In the original setup, the tracer spreads through an external ring following the vortex described in Figures 3, 4 and 5; under all the different rheologies, the stagnant zone at the centre (in black) is clearly evident.

In both the nozzle-switching configurations, the tracer becomes almost uniform throughout the domain, despite the above-mentioned attenuation of the velocity flow patters. The average value of χ evidently changes depending on rheology and switching interval, and some minor differences in tracer distribution can be observed; however, in all the cases, the stagnant zone at the centre of the domain vanishes completely. Such cancellation of the central dead zones is a critical benefit of the switching strategy, confirming the benefits to be derived from the introduction of the additional nozzle series.

4 Conclusions

For the first time, an Euler-Lagrangian CFD model was used to model gas mixing in a full-scale anaerobic digester.

The traditional approach to assess mixing quality, based on evaluating the average shear rate, was shown to be inapplicable to the case of full-scale, gas-mixed digesters. As an alternative, two novel approaches, based on the analysis of shear rate relative intensity intervals, and the introduction of a passive, non-diffusive scalar tracer, were evaluated.

The formation of low viscosity flow patterns under certain mixing conditions was observed and their detrimental effect on mixing were discussed.

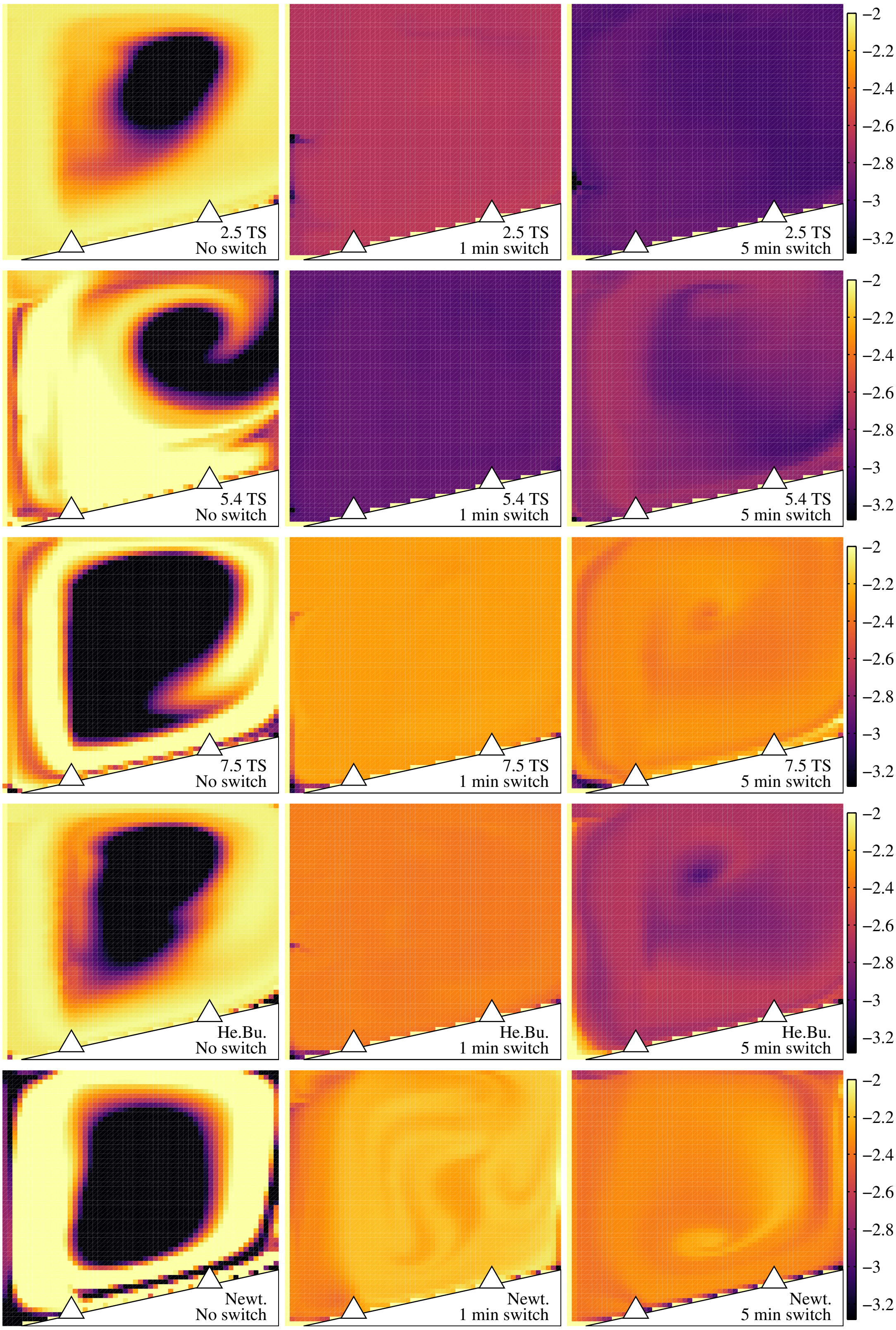

Figure 13: $\log_{10} \chi$ for $q = 0.5$ after 1,200 s.

A new strategy to improve mixing quality was introduced. Specifically, it consists of arranging a second series of nozzles at a different distance from the tank symmetry axis, and switching biogas injection between the original and the new series at regular time intervals. This strategy was shown to be successful in removing the dead zones at the centre of the tank, irrespective of the sludge rheology, when switching was performed every minute or every five minutes.

Even without applying the above-mentioned strategy, the CFD results show that the quality of mixing is not expected to drop significantly when the maximum gas flow rate in the study presented here is halved. More generally, the power per unit volume can be lowered down to approximately $1\ \mathrm{W\,m^{-3}}$, thus saving half of the reference input power for this study corresponding to $q = 1$, for the same expected biogas yield. Further research aimed at implementing viscosity flow patterns mitigation strategies is required to demonstrate that even higher input mixing power savings are achievable without changes in the biogas yield.

The flow patterns depend on bubble size, and therefore further research aimed at experimentally measuring bubble size in gas-mixed digesters is desirable. Nevertheless, the shear rate dependence over total solid and mixing input power show similar trends for all the bubble sizes considered, and therefore the conclusions drawn hold irrespective of the bubble size.

Acknowledgments

The details of the digester geometry were kindly provided by Peter Vale and Severn Trent Water Ltd., whom the authors gratefully acknowledge.
The computational work reported in this paper was undertaken using the BlueBEAR high performance computing facility at the University of Birmingham, UK. The authors are grateful for the facility and support provided by the University.
The first author is funded via a University of Birmingham Postgraduate Teaching Assistantship award.

References

[1] D. Dapelo, J. Bridgeman, "Computational Fluid Dynamics Modelling of Unconfined Gas Mixing of Wastewater Sludge in a Full Scale Anaerobic Digester", in *Civil-Comp Proceedings*, Volume 108. Civil-Comp Press, 2015, ISSN 17593433, doi:10.4203/ccp.108.270.

[2] P.J. Roache, "Verification of codes and calculations", *AIAA Journal*, 36(5): 696–702, 1998, ISBN 0001-1452, ISSN 0001-1452, doi:10.2514/3.13882.

[3] Council of the European Union, "Council Directive of 21 May 1991 concerning Urban Waste Water Treatment (91/271/EEC)", 1991, ISBN 9789279122552.

[4] European Environment Agency, “Waterbase - UWWTD: Urban Waste Water Treatment Directive reported data”, Technical report, 2015.

[5] Ofwat, “Towards Water 2020 meeting the challenges for water and wastewater services in England and Wales”, Technical report, Birmingham (UK), 2015.

[6] WWAP (World Water Assessment Programme), “The United Nations World Water Development Report 4: Managing Water under Uncertainty and Risk”, Technical report, UNESCO, Paris, 2012, ISBN 978-92-3-104235-5.

[7] P.G. Stroot, K.D. McMahon, R.I. Mackie, L. Raskin, “Anaerobic codigestion of municipal solid waste and biosolids under various mixing conditionsI. digester performance”, *Water Research*, 35(7): 1804–1816, may 2001, ISBN 0043-1354, ISSN 00431354, doi:10.1016/S0043-1354(00)00439-5.

[8] K.D. McMahon, P.G. Stroot, R.I. Mackie, L. Raskin, “Anaerobic codigestion of municipal solid waste and biosolids under various mixing conditions-II: Microbial population dynamics”, *Water Research*, 35(7): 1817–1827, 2001, ISBN 0043-1354, ISSN 00431354, doi:10.1016/S0043-1354(00)00438-3.

[9] H.K. Ong, P.F. Greenfield, P.C. Pullammanappallil, “Effect of Mixing on Biomethanation of Cattle-Manure Slurry”, *Environmental Technology*, 23(10): 1081–1090, oct 2002, ISSN 0959-3330, doi:10.1080/09593332308618330.

[10] X. Gómez, M.J. Cuetos, J. Cara, a. Morán, a.I. García, “Anaerobic co-digestion of primary sludge and the fruit and vegetable fraction of the municipal solid wastes. Conditions for mixing and evaluation of the organic loading rate”, *Renewable Energy*, 31(12): 2017–2024, 2006, ISBN 0960-1481, ISSN 09601481, doi:10.1016/j.renene.2005.09.029.

[11] A.J. Ward, P.J. Hobbs, P.J. Holliman, D.L. Jones, “Optimisation of the anaerobic digestion of agricultural resources”, *Bioresource Technology*, 99(17): 7928–7940, 2008, ISBN 0960-8524, ISSN 09608524, doi:10.1016/j.biortech.2008.02.044.

[12] J. Bridgeman, “Computational fluid dynamics modelling of sewage sludge mixing in an anaerobic digester”, *Advances in Engineering Software*, 44(1): 54–62, 2012, ISSN 09659978, doi:10.1016/j.advengsoft.2011.05.037.

[13] R.C. Sindall, J. Bridgeman, C. Carliell-Marquet, “Velocity gradient as a tool to characterise the link between mixing and biogas production in anaerobic waste digesters”, *Water Science and Technology*, 67(12): 2800–2806, 2013, ISBN http://www.iwaponline.com/wst/06712/wst067122800.htm, ISSN 02731223, doi:10.2166/wst.2013.206.

[14] B. Wu, "CFD simulation of gas and non-Newtonian fluid two-phase flow in anaerobic digesters", *Water Research*, 44(13): 3861–3874, 2010, ISSN 00431354, doi:10.1016/j.watres.2010.04.043.

[15] M.S. Vesvikar, M.H. Al-Dahhan, "Flow pattern visualization in a mimic anaerobic digester using CFD", *Biotechnology and Bioengineering*, 89(6): 719–732, 2005, ISSN 00063592, doi:10.1002/bit.20388.

[16] K. Karim, G.J. Thoma, M.H. Al-Dahhan, "Gas-lift digester configuration effects on mixing effectiveness", *Water Research*, 41(14): 3051–3060, 2007, ISSN 00431354, doi:10.1016/j.watres.2007.03.042.

[17] R.N. Meroney, P.E. Colorado, "CFD simulation of mechanical draft tube mixing in anaerobic digester tanks", *Water Research*, 43(4): 1040–1050, 2009, ISSN 00431354, doi:10.1016/j.watres.2008.11.035.

[18] M. Terashima, R. Goel, K. Komatsu, H. Yasui, H. Takahashi, Y.Y. Li, T. Noike, "CFD simulation of mixing in anaerobic digesters", *Bioresource Technology*, 100(7): 2228–2233, 2009, ISBN 0960-8524, ISSN 09608524, doi:10.1016/j.biortech.2008.07.069.

[19] K.J. Craig, M.N. Nieuwoudt, L.J. Niemand, "CFD simulation of anaerobic digester with variable sewage sludge rheology", *Water Research*, 47(13): 4485–4497, 2013, ISBN 1879-2448 (Electronic) 0043-1354 (Linking), ISSN 00431354, doi:10.1016/j.watres.2013.05.011.

[20] F. Hurtado, A. Kaiser, B. Zamora, "Fluid dynamic analysis of a continuous stirred tank reactor for technical optimization of wastewater digestion", *Water Research*, 71: 282–293, 2015, ISSN 00431354, doi:10.1016/j.watres.2014.11.053.

[21] C.E. Brade, G.P. Noone, "Anaerobic sludge digestion: Need it be expensive? Making more of existing resources", 1981, ISSN 0043129X.

[22] B. Wu, "Integration of mixing, heat transfer, and biochemical reaction kinetics in anaerobic methane fermentation", *Biotechnology and Bioengineering*, 109 (11): 2864–2874, 2012, ISBN 0006-3592, ISSN 00063592, doi:10.1002/bit.24551.

[23] B. Wu, "CFD simulation of gas mixing in anaerobic digesters", *Computers and Electronics in Agriculture*, 109: 278–286, nov 2014, ISSN 01681699, doi:10.1016/j.compag.2014.10.007.

[24] B. Andersson, R. Andersson, L. Håkansson, M. Mortensen, N. Defence, R. Sudiyo, B. van Wachem, *Computational Fluid Dynamics for Engineers*, Cambridge University Press, 2012, ISBN 9781139093590.

[25] D. Dapelo, F. Alberini, J. Bridgeman, "Euler-Lagrange CFD modelling of unconfined gas mixing in anaerobic digestion", *Water Research*, 85: 497–511, 2015, ISSN 00431354, doi:10.1016/j.watres.2015.08.042.

[26] R.C. Sindall, D. Dapelo, T. Leadbeater, J. Bridgeman, "Positron emission particle tracking (PEPT): A novel approach to flow visualisation in lab-scale anaerobic digesters", *Flow Measurement and Instrumentation*, 54: 250–264, 2017, ISSN 09555986, doi:10.1016/j.flowmeasinst.2017.02.009.

[27] B. Wu, "CFD simulation of mixing in egg-shaped anaerobic digesters", *Water Research*, 44(5): 1507–1519, 2010, ISSN 00431354, doi:10.1016/j.watres.2009.10.040.

[28] B. Wu, "CFD investigation of turbulence models for mechanical agitation of non-Newtonian fluids in anaerobic digesters", *Water Research*, 45(5): 2082–2094, 2011, ISSN 00431354, doi:10.1016/j.watres.2010.12.020.

[29] B. Wu, "CFD simulation of mixing for high-solids anaerobic digestion", *Biotechnology and Bioengineering*, 109(8): 2116–2126, 2012, ISSN 00063592, doi:10.1002/bit.24482.

[30] A. Achkari-Begdouri, P.R. Goodrich, "Rheological properties of Moroccan dairy cattle manure", *Bioresource Technology*, 40: 225–233, jan 1992, ISBN 0960-8524, ISSN 09608524, doi:10.1016/0960-8524(92)90201-8.

[31] N. Eshtiaghi, F. Markis, S.D. Yap, J.C. Baudez, P. Slatter, "Rheological characterisation of municipal sludge: A review", *Water Research*, 47(15): 5493–5510, 2013, ISSN 00431354, doi:10.1016/j.watres.2013.07.001.

[32] B. Wu, S. Chen, "CFD simulation of non-Newtonian fluid flow in anaerobic digesters", *Biotechnology and Bioengineering*, 99(3): 700–711, 2008, ISSN 00063592, doi:10.1002/bit.21613.

[33] H. Landry, C. Laguë, M. Roberge, "Physical and rheological properties of manure products", *Applied Engineering in Agriculture*, 20(3): 277–288, 2004, ISBN 0883-8542, ISSN 08838542, doi:10.13031/2013.16061.

[34] P.S. Monteiro, "The influence of the anaerobic digestion process on the sewage sludges rheological behaviour", *Sludge Rheology Selected Proceedings of the International Workshop on the Rheology of Sludges Sludge Management International Specialized Conference on Sludge Management*, 36(11): 61–67, 1997, ISSN 0273-1223, doi:10.1016/S0273-1223(97)00670-7.

[35] J.C. Baudez, P. Slatter, N. Eshtiaghi, "The impact of temperature on the rheological behaviour of anaerobic digested sludge", *Chemical Engineering Journal*, 215-216: 182–187, 2013, ISBN 1385-8947, ISSN 13858947, doi:10.1016/j.cej.2012.10.099.

[36] E.L. Paul, V.A. Atiemo-Obeng, S.M. Kresta, *Handbook of Industrial Mixing: Science and practice*, John Wiley & Sons, Inc., Hoboken, NJ, USA, 2004, ISBN 0-471-26919-0, ISSN 0883-7554, doi:10.1002/0471451452.ch8.

[37] K. Dewsbury, D. Karamanev, a. Margaritis, "Hydrodynamic characteristics of free rise of light solid particles and gas bubbles in non-Newtonian liquids", *Chemical Engineering Science*, 54(21): 4825–4830, 1999, ISSN 00092509, doi:10.1016/S0009-2509(99)00200-6.

[38] A. Tomiyama, H. Tamai, I. Zun, S. Hosokawa, "Transverse migration of single bubbles in simple shear flows", *Chemical Engineering Science*, 57(11): 1849–1858, 2002, ISSN 00092509, doi:10.1016/S0009-2509(02)00085-4.

[39] M.M. Gibson, B.E. Launder, "Ground effects on pressure fluctuations in the atmospheric boundary layer", *Journal of Fluid Mechanics*, 86: 491–511, 1978, ISSN 0022-1120, doi:10.1017/S0022112078001251.

[40] B.G.M. van Wachem, A.E. Almstedt, "Methods for multiphase computational fluid dynamics", *Chemical Engineering Journal*, 96(1-3): 81–98, 2003, ISBN 1385-8947, ISSN 13858947, doi:10.1016/j.cej.2003.08.025.

[41] R. Sungkorn, J.J. Derksen, J.G. Khinast, "Modeling of turbulent gas-liquid bubbly flows using stochastic Lagrangian model and lattice-Boltzmann scheme", *Chemical Engineering Science*, 66(12): 2745–2757, 2011, ISBN 0009-2509, ISSN 00092509, doi:10.1016/j.ces.2011.03.032.

[42] R. Sungkorn, J.J. Derksen, J.G. Khinast, "Modeling of aerated stirred tanks with shear-thinning power law liquids", *International Journal of Heat and Fluid Flow*, 36: 153–166, 2012, ISBN 0142-727X, ISSN 0142727X, doi:10.1016/j.ijheatfluidflow.2012.04.006.

[43] T.R. Camp, P.C. Stein, "Velocity gradients and internal work in fluid motion", *Journal of the Boston Society of Civil Engineering*, 85: 218–237, 1943.

[44] M.M. Clark, "Critique of Camp and Stein's RMS Velocity Gradient", *Journal of Environmental Engineering*, 111(6): 741–754, dec 1985, ISSN 0733-9372, doi:10.1061/(ASCE)0733-9372(1985)111:6(741).

[45] G. Tchobanoglous, L. Burton, Franklin, H.D. Stensel, *Wastewater Engineering*, Metcalf & Eddy, Inc, 2010, ISBN 7-302-05857-1, pages 1–1878.

[46] U.S. EPA, "Process Design Manual for Sludge Treatment and Disposal", Technical report, U.S. Environmental Protection Agency, Cincinnati, OH, 1979.